RSC Advances




ROYAL SOCIETY OF CHEMISTRY

www.rsc.org/advances

Cite this: DOI: 10.1039/c0xx00000x

www.rsc.org/xxxxxx

ARTICLE

# Optically and magnetically doped ormosil nanoparticles for bioimaging: synthesis, characterization, and *in vitro* studies

**Pramod Kumar, Anuradha, and Indrajit Roy**

***Received (in XXX, XXX) Xth XXXXXXXXX 20XX, Accepted Xth XXXXXXXXX 20XX***
**DOI: 10.1039/b000000x**

In this manuscript, we report the fabrication of a dual-modality nanoprobe involving co-encapsulation of fluorophore and iron-oxide nanoparticles within ormosil nanoparticles, and their applications in *in vitro* bioimaging. The entire synthesis, including microwave-mediated precipitation of the iron-oxide nanoparticles, was carried out within the non-aqueous core of oil-in-water microemulsion. The nanoparticles are spherical and monodispersed, with average diameter around 150 nm. After synthesis, their composition, stability, crystallinity, as well as magnetic and optical properties were evaluated. X-ray diffraction studies of the non-encapsulated iron oxide nanoparticles showed them to be crystalline, corresponding to the α-$Fe_2O_3$ phase. However, their crystallinity was found to diminish upon ormosil encapsulation. These doped nanoparticles displayed both optical and superparamagnetic properties, by virtue of which they have the potential to serve as dual diagnostic probes. The stability of the fluorophore was found to increase upon nanoencapsulation. *In vitro* studies have shown that the nanoparticles are non-toxic to cells in culture; with efficient cellular uptake, as shown by optical bioimaging. These observations underscore the promise of such nanoparticles in non-toxic bioimaging applications.

## Introduction

Among the various diagnostic techniques presently available at the clinical and pre-clinical setting, such as magnetic resonance imaging (MRI), ultrasound, radioimaging, x-ray imaging, optical imaging, etc., no single technique alone can facilitate comprehensive diagnostic visualization about a diseased cell/tissue/organ.[1-3] This realization has fuelled research towards the development of multimodal diagnostic probes, that will facilitate combination diagnostics, preferably covering both the anatomical and physiological aspects of a disease.[4,5]

Nanoparticles, owing to their small size and size-dependent unique properties, present ideal platforms for the fabrication of multimodal agents.[6-10] Such multimodal agents are expected to play a leading role in medical diagnostics in the future. Two kinds of nanoparticles have been categorized based on their applications, which are (a) functional nanoparticles with some unique physical parameter, such as iron oxide and metallic nanoparticle, quantum dots, etc., and (b) structural nanoparticles, such as silica, biodegradable polymers, etc., which provide a matrix for hosting one/multiple active agent/s, including smaller functional nanoparticles. Moreover, their surfaces can be aptly functionalized to provide them with enhanced blood-circulation and targeting specificity.[11-13]

Among the various kinds of functional nanoparticles available, iron-oxide nanoparticles perhaps have the most promising applications in the field of medicine.[14-17] Their ultrasmall size, superparamagnetic properties, ease of synthesis, and biocompatibility makes them ideally suited for a variety of medical applications. Their most important applications are contrast enhancement in magnetic resonance imaging (MRI) and provision for magnetically guided drug delivery.[18,19] Their use in magnetic field assisted triggering of local hyperthermia for localized anticancer activity has also been demonstrated.[20,21] Moreover, they have been found to be largely biocompatible and non-toxic. Despite these benefits, iron oxide nanoparticles have limited applicability for *in vitro* bioimaging studies.

It has been proposed that a hybrid diagnostic agent comprising of iron oxide nanoparticle and optical probe will have the dual capability of MRI and high-resolution optical imaging.[1] Dual magnetic and optical probes using organic fluorophores conjugated on the surface of iron-oxide nanoparticles have been reported.[22] However, such a design leads to modification of the iron-oxide surface with the fluorophores, thereby altering their biodistribution and other pharmacological parameters. Moreover, the exposed fluorophore may get degraded or quenched in the physiological milieu. Therefore, co-encapsulation of iron-oxide nanoparticles and fluorophores within inert, mesoporous nanostructures is an alternative strategy for preserving the magnetic and optical properties for potential bi-modal bioimaging.

One of the most simple and yet versatile structural nanomaterials is made up of organically modified silica (ormosil).[23] Highly monodispersed ormosil nanoparticles, encapsulating poorly water-soluble molecules, can be easily synthesized in the oil-in-water microemulsion media.[24]

Encapsulation of active molecules within these nanoparticle matrixes ensures that (a) the encapsulants are protected from environmental insult, and (b) the nanoparticle surface can be further modified for a specific application. Therefore, these doped nanoparticles have found a variety of applications, such as drug delivery in photodynamic therapy (PDT), gene therapy, optical bioimaging, etc.[25-27] Their non-toxicity and biocompatibility has also been indicated in cultured cells, small animals, and drosophila.[28-30] Moreover, their surfaces have been functionalized to incorporate inert polymers and biorecognition agents for enhanced bioavailability and target specificity.[27] Taken together, ormosil nanoparticles are well suited for providing robust platforms for the fabrication of multimodal nanoparticles.

In this work, we have used an one-pot method for the synthesis of ormosil nanoparticles, co-encapsulating iron-oxide nanoparticle and an organic fluorophore, for providing combined MRI and optical imaging capabilities, respectively. The iron oxide nanoparticles were synthesized in the oil-in-water microemulsion media by the microwave-assisted decomposition of the oil-soluble precursor, ferric acetylacetonate. Next, these magnetic nanoparticles, along with a fluorophore [nile-red or ruthenium-*tris*(2,2′-bipyridyl) dichloride], were co-encapsulated within ormosil nanoparticles by alkaline hydrolysis of corresponding organosilane precursor. The resulting nanoparticles were characterized for their size, composition, functionality, crystallinity, along with their magnetic and optical behaviour. The stability of the nanoencapsulated fluorophore *vis-a-vis* that of free fluorophore has also been investigated. Following that, they were treated with cultured cells to probe their non-toxicity and biocompatibility. Concurrently, their uptake in cells in culture was studied by optical bioimaging. The purpose of the above structural, functional, and preliminary *in vitro* investigations was to explore their potential usefulness for advanced biomedical imaging in the future.

## Experimental

### Materials:

The surfactants aerosol OT (AOT), co-surfactant 1-butanol, the ormosil precursor vinyltriethoxysilane (VTES), fluorophores nile-red (NR) and ruthenium-*tris*(2,2′-bipyridyl) dichloride (RU), and the MTT reagent were purchased from Sigma-Aldrich. Cell culture reagents were obtained from Invitrogen. The lung carcinoma cells lines (MCF-7) was purchased from ATCC, VA, and cultured according to instructions supplied by the vendor. Ferric acetylacetonate is a product of Alfa Aesar. Unless otherwise mentioned, all other cell culture products were obtained from Thermo Fisher Scientific. All chemicals were used without any further purification. Unless otherwise mentioned, the experiments were carried out at ambient temperature and pressure. Doubly distilled water was used throughout the experiments.

### Microwave assisted synthesis of iron oxide (IO) nanoparticles in micellar media:

The nanostructures were synthesized in the non-aqueous core of an oil-in-water microemulsion system.[24] Briefly, the microemulsion was prepared by dissolving 0.22 g of the surfactant AOT in 10 mL of water, along with 400µL of the co-surfactant 1-butanol. To this system, 300 µL of ferric acetylacetonate in DMSO (0.1M) was added and the solution was vigorously stirred for 1 hour. The resulting clear solution with light-brown colour was transferred to a microwave reaction vessel equipped with a stir bar. [31] The solution, under rapid stirring, was heated to $50^0$C and irradiated with microwave (300 W maximum power, 100 psi maximum pressure) for 10 min, after which it was removed from the microwave chamber and kept at room temperature for further reaction. The colour of the solution changed to brown after microwave irradiation.

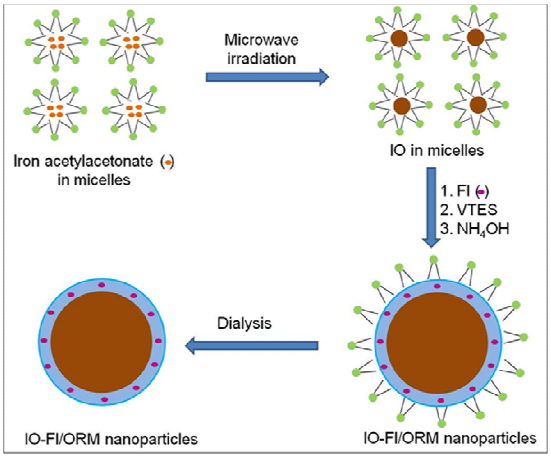


***Scheme 1: Schematics of one-pot synthesis of ormosil nanoparticles co-encapsulating iron-oxide nanoparticle and fluorophore (IO-Fl/ORM; Fl = NR or RU).***

### Synthesis of iron oxide and fluorophore encapsulated in ormosil (ORM) nanostructures (IO-Fl/ORM; Fl: NR or RU):

Following the microwave assisted synthesis of iron oxide nanoparticles in the miceller core, they, along with the fluorophore (NR or RU), were encased within ormosil nanoparticles in the same reaction vessel. Briefly, to the brown coloured microemulsion solution, 300 µL of NR in DMSO (3.14 mM) were added under vigorous magnetic stirring. Alternately, for encapsulating RU, a 4 mM solution of the fluorophore in DMSO was added. After that, to the solution, 100 µL of neat vinyltriethoxysilane (VTES) was added, and vigorously stirred for further one hour. After this period, 10 µL of each of aqueous ammonia solution and neat 3-aminopropyltriethoxysilane (APTES) were added to the solution, and left for overnight stirring for the formation of the nanostructures. Following the synthesis, the surfactant, co-surfactant, and other unreacted molecules were removed by dialysis against distilled water for about 48 hours, using a cellulose dialysis membrane with a cut-off size of 12–14 kDa. At the end of dialysis, the nanostructures were sterile filtered using 0.45 µm syringe filter, and one portion was stored at 4 °C for future use. The other portion was centrifuged, and the pink-brown precipitate formed was washed twice, oven dried and stored as powder. The synthesis procedure is shown in Scheme 1.

### Characterization:

The sizes of the iron-oxide nanoparticles, before and after encapsulation within ormosil nanoparticles, were determined using transmission electron microscopy (TEM). For TEM, the aqueous dispersions were sonicated, drop-coated and dried onto

formvar coated 200 mesh copper grids (Ted Pella, USA), followed by imaging using a TECNAI $G^2$-30 U TWIN TEM instrument (FEI, Eindhoven, The Netherlands) with an acceleration voltage of 300 kV. The same instrumentation setup was used for probing the crystalline diffraction pattern (using selected area electron diffraction, or SAED) of the nanoparticles.

The sizes of the nanoparticles were further analyzed by dynamic light scattering (DLS) measurements. Here, aqueous-dispersed samples of the nanoparticles were taken in glass cuvettes, and analysed using a NANO-ZS series MALVERN ZETASIZER instrument. A He-Ne laser (wavelength 633nm, power 4mW) was used as the light source. Number average hydrodynamic size distribution of nanoparticles were plotted.

The magnetic properties of the dried nanoparticles were probed using vibrating sample magnetometer (VSM), using a Model 3473-70 electromagnet amplifier (CREST Performance CPX 900 power amplifier Instrument). High resolution powder X-ray diffraction (XRD) was used to analyze the phase composition of the nanoparticles, using a Brukar $D_8$ Discover X-ray spectrometer, over the 2θ° range from 20–$65^0$ at rate of 2.58/min, using Cu-Kα radiation (λ= 1.54060 A˚).

The optical properties (UV-visible absorption and fluorescence emission spectra) of the various aqueous nanoparticulate samples, both with and without NR or RU, were recorded using a Shimadzu UV-1601 spectrophotometer (Shimadzu, Kyoto, Japan) and a Cary Eclipse fluorescence spectrometer (Varian, Palo Alto, CA), respectively.

The stability of the fluorophore RU, both free and nanoencapsulated, were studied using fluorescence quenching experiment. Here, fixed concentrations of free and nanoencapsulated fluorophore in aqueous medium have been treated with various concentrations of the chemical quencher $Cu^{2+}$ (copper sulfate).[32] Fluorescence emission intensities in the absence (Io) and presence (I) of various quencher concentrations was then measured using the Cary Eclipse fluorescence spectrophotometer. A plot was made with the natural log of (I/Io) versus quencher concentration [Q]. The slope of the plot correlated directly with the magnitude of chemical quenching of the fluorophore.

In addition, the fluorescence decay spectra of the free and nanoencapsulated fluorophore was obtained using time-correlated single photon counting (TCSPC) technique.[33] The samples were excited with NanoLED 460 pulsed diode (Horiba, Jovin Yvon), at excitation wavelength of 460 nm and pulse duration FWHM of 1.4 ns. Single photon detection was carried out using the TBX-04 (Horiba, Jovin Yvon) picosecond photon-detection module, along with FluoroHub (Horiba) timing electronics. Decay analysis was done using DAS6 software.

***In vitro* studies**:

The human breast cancer cells MCF-7 were grown in DMEM media, supplemented with 10% fetal bovine serum (FBS), 1% antibiotic penicillin/streptomycin, and 1% antifungal Amphotericin B. The cells were maintained at 37 °C, 5% $CO_2$ in a humidified incubator, using standard cell culture procedures and manufacturer's instructions.

For analyzing cell viability upon treatment with various nanoparticles, one day prior to treatment, the cells were trypsinized and resuspended in fresh media. 1,00,000 cells/1 mL fresh media were added to each well of a sterilized 24-well plate, and transferred back to the incubator for attachment and overnight growth. Next day, to the cells at a confluency of 70–80%, three different dosages of the various samples were added, mixed by swirling, and transferred back to the incubator. The added samples were fluorophore NR, iron oxide (IO) nanoparticles, as well as IO and NR co-encapsulated ormosil nanoparticles (IO-NR/ORM). After three days of incubation, the plate was taken out, and the cells in each well were washed three times with sterile PBS, and treated with 100 µL of MTT reagent [3-(4,5-dimethylthiazol-2-yl)-2,5-diphenyltetrazolium bromide, (5 mg/mL in PBS)] for 2 hours.[24] The resulting blue-coloured formazan crystals were dissolved in DMSO, and the optical density of this solution was recorded at 570 nm using UV–visible spectrophotometry. The optical density of each solution reflected the viability of the cells in each well. The percentage viability of the treated cells were calculated after comparing their optical density with that of non-treated cells (positive control), the later being arbitrarily assigned 100 % viability. The experiment was carried out in triplicates for statistical significance.

For monitoring the uptake of the fluorophore-doped nanoparticles in cells, one day prior to treatment, the cells were seeded in sterilized 6-well plate (2,00,000 cells/2 mL fresh media in each well) and returned to the incubator. Next day, to the cells at a confluency of 70–80%, three dosages of the various samples were added, mixed by swirling, and returned to the incubator for two hours. After incubation, the plate was taken out, the cells in each well washed twice with sterile PBS, and fixed by a mixture of methanol and glycerol. The fixed cells were visualized under a fluorescent Nikon TS-100 inverted microscope, and photographed using a Nikon DIGITAL SIGHT DS-Fi1 Camera (Nikon, Japan).

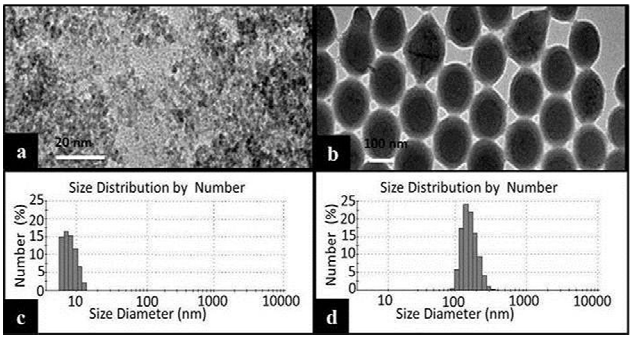


***Fig. 1: (a, b) TEM images of (a) free iron oxide nanoparticles (IO; scale bar: 20 nm), and (b) ormosil nanoparticles co-encapsulating iron-oxide nanoparticles and NR (IO-NR/ORM; scale bar: 100 nm). (c, d) DLS data showing hydrodynamic diameters (number average size distribution) of aqueous dispersions of (c) IO, and (d) IO-NR/ORM nanoparticles.***

## Results and discussions

The TEM images of the synthesized iron-oxide nanoparticles, before (IO) and after co-encapsulation with NR within ormosil nanoparticles (IO-NR/ORM), are shown in Fig. 1. The non-encapsulated IO nanoparticles are irregular and grain shaped, with an average size of about 4 nm (Fig. 1a). Figure 1b represents the IO-NR/ORM nanoparticles, with a clearly discernible core-

shell architecture, with the more electron dense IO forming the 'dark' core, and ormosil forming the 'light' shell. The average overall diameter is about 150 nm, with an average core diameter of about 120 nm, with reasonable size uniformity in each case. A simple visual comparison with the free IO nanoparticles shows that several IO nanoparticles have aggregated upon encapsulation within the ormosil matrix. This kind of aggregation is also seen in ormosil nanoparticles encapsulating only IO, without co-encapsulated fluorophore (IO/ORM; data not shown), which indicates that the fluorophore plays no role in this observed IO aggregation.

Their sizes have been further determined by dynamic light scattering (DLS), which measures the hydrodynamic diameter. Fig. 1(c) and 1 (d) presents the DLS data of IO and IO-NR/ORM, respectively, with respective mean hydrodynamic diameters of 8 nm and 155 nm. The DLS data agrees well with the TEM results. Overall, the sizes of IO-NR/ORM nanoparticles are reasonably small (diameter around 150 nm) and monodispersed.

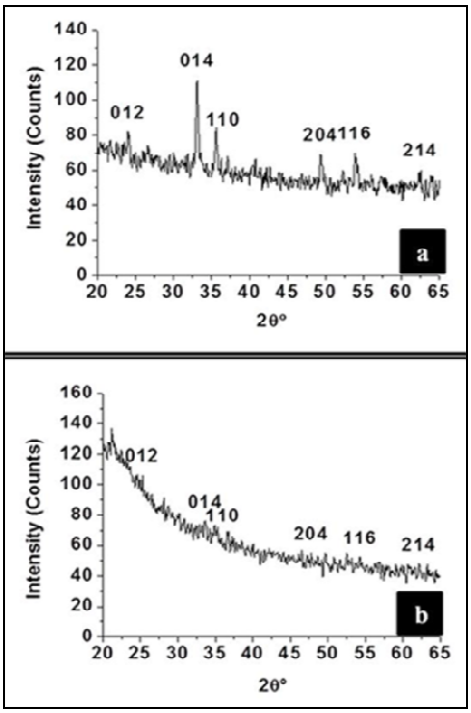


***Fig. 2: Powder X-ray diffraction (XRD) spectra of (a) free iron oxide nanoparticles (IO), and (b) ormosil nanoparticles co-encapsulating iron-oxide nanoparticles and nile-red (IO-NR/ORM).***

Fig. 2a represents the powder XRD spectrum of the IO nanoparticles, showing diffraction peaks of (012), (014), (110), (113), (024), (116), (214) and (300), which match the characteristic peaks of $\alpha$-$Fe_2O_3$ (Hematite, JCPDS86-0550).[34] The sharpness of XRD peaks indicated the crystalline nature of the nanostructures. In comparison, for the XRD spectrum of IO-NR/ORM nanoparticles (Fig. 2b), the peaks appeared highly diminished, demonstrating that the crystalline IO nanoparticles have been shielded by a layer of amorphous ormosil matrix. This crystalline pattern is also observed from the SAED data (ESI, Fig. S1†).

Fig. 3 shows the magnetization curves of the IO and IO-NR/ORM nanoparticles, measured at room temperature using vibrating sample magnetometry (VSM). Under a large external field, the magnetization of the particles aligns with the field direction and reaches its saturation value for both these nanoparticles. The pattern is typical of superparamagnetic nanoparticles.[35] The saturation magnetization (Ms) values of IO and IO-NR/ORM nanoparticles were 1.0 and 0.80 emu/g, respectively. This result shows that co-encapsulation with fluorophore within ormosil nanoparticles did not significantly alter the magnetic behaviour of IO nanoparticles.

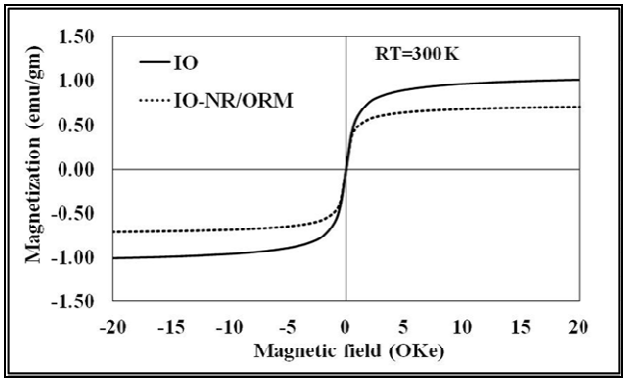


***Fig. 3: Magnetization (VSM) curves of free iron oxide nanoparticles (IO; solid line), and ormosil nanoparticles co-encapsulating iron-oxide nanoparticles and nile-red (IO-NR/ORM; broken line).***

The optical properties of the various samples have been studied by UV-visible and fluorescence spectroscopies. Fig. 4a shows the absorption spectrum of IO nanoparticles, formed after microwave irradiation of ferric acetylacetonate dissolved in micelles. For comparison, the spectra of ferric acetylacetonate, dissolved in DMSO, as well as within micelles prior to microwave irradiation, are also provided. It can be seen that the characteristic absorption peaks of ferric acetylacetonate, which are observed around 360 nm and 434 nm, disappear after microwave irradiation, indicating the decomposition of this compound and formation of nanoparticles. Fig. 4b shows the absorption spectrum of IO-NR/ORM nanoparticles. For comparison, the spectra of NR/micelles, and IO-NR/micelles (after microwave irradiation), are also provided. It can be seen that the characteristic absorption peak of NR (around 560 nm) is substantially diminished after co-encapsulation with IO within micelles, as well as within ORMOSIL nanoparticles. This can be partially attributed to the shielding of the nile-red absorption by scattering from IO and ormosil nanoparticles, as well as some optical quenching by IO. Nevertheless, the presence of nile-red in the nanoparticulate samples is ascertained from their fluorescence emission spectra. Fig. 4c shows the fluorescence spectra of NR in micelles, IO-NR in micelles, and IO-NR/ORM nanoparticles, each excited at 560 nm. The data shows the characteristic emission of NR in each case; although the peak intensity of NR is diminished and red-shifted upon nanoencapsulation. Similar optical data was observed in the case of IO-RU/ORM nanoparticles (ESI, Fig. S2†).

The motivation of encapsulating fluorophores within transparent nanomaterials is to enhance the optical stability of the fluorophores. We probed whether nanoencapsulation enhances

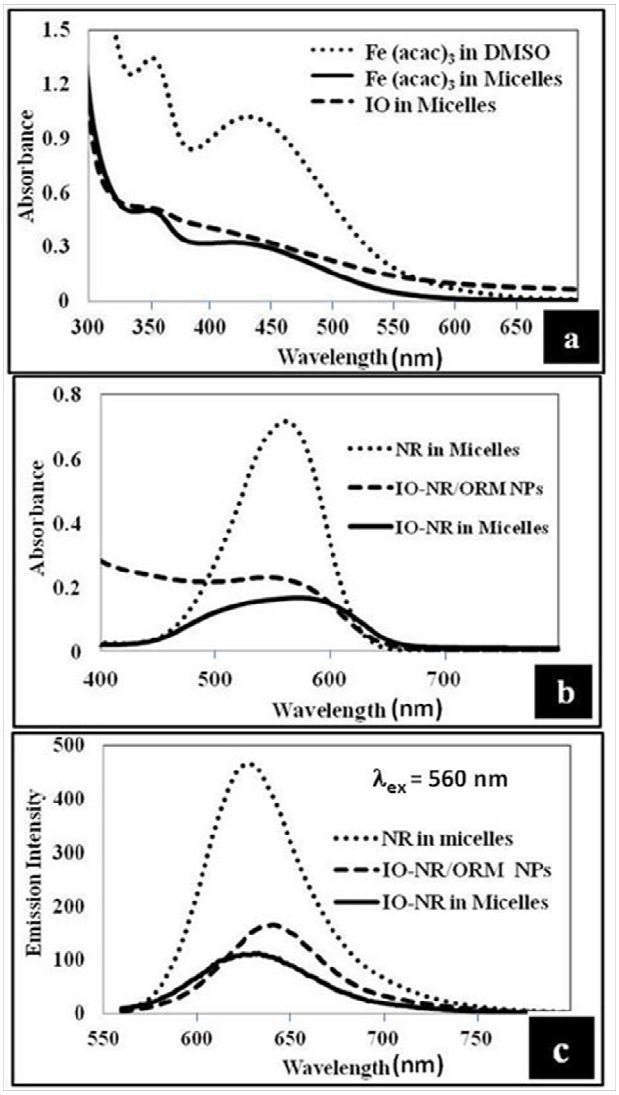


***Fig. 4: (a) Comparative absorption spectra of ferric acetylacetonate in micelles, and iron-oxide nanoparticles (IO) in micelles formed after microwave irradiation of the former. The absorption spectrum of ferric acetylacetonate in DMSO (no microwave irradiation) is also shown as a reference. (b) Absorption spectrum of iron-oxide nanoparticles and NR fluorophore co-encapsulated within micelles, as well as within ormosil nanoparticles. The absorption spectrum of NR dissolved in micelles is also shown for comparison. (c) Fluorescence emission spectrum of iron-oxide nanoparticles and NR fluorophore co-encapsulated within micelles, as well as within ormosil nanoparticles. The emission spectrum of NR dissolved in micelles is also shown for comparison.***

the stability of fluorophores, using chemically-induced fluorescence quenching experiment. From Fig. 5(a), it is clear that the free fluorophore is more sensitive to chemical quenching than the nanoencapsulated fluorophore, as the free fluorophore has steeper fluorescence quenching curve. This indicates the enhanced stability of nanoencapsulated fluorophore. The result of fluorescence decay experiment is given in Fig. 5(b), showing exponential decay curve for both free and nanoencapsulated fluorophore. However, the free fluorophore has a steeper fluorescence decay curve, and hence lesser fluorescence lifetime, when compared to that of the nanoencapsulated fluorophore. This result indicates that fluorescence lifetime is increased upon nanoencapsulation. These results demonstrate that albeit the

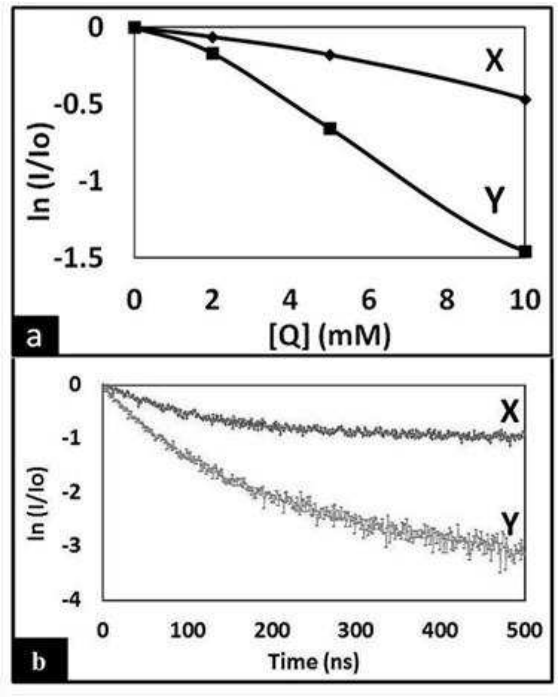


***Fig. 5: (a) Chemically-induced fluorescence quenching data of fluorophore Ru, (x) co-encapsulated with IO within ormosil nanoparticles, and (y) in free form. (b) Time-resolved fluorescence decay data of fluorophore Ru, (x) co-encapsulated with IO within ormosil nanoparticles, and (y) in free form.***

fluorescence intensity diminished for the nanoencapsulated fluorophore, it became more photostable with enhanced fluorescence lifetime. Overall, these optical data, along with the magnetism data from fig. 3, show that the dually-doped ormosil nanoparticles show both magnetic and optical behaviour. Thus, they are promising bi-modal contrast agents for efficient biomedical imaging.

Finally, in order to study the biocompatibility and non-cytotoxicity of the various nanoparticles, we have treated live cells with these nanoparticles and analyzed the cell viability. It can be seen from Fig. 6a that after 72 hours of nanoparticle-treatment at various dosages, the cells remained more than 90 % viable, even at a dosage as high as 1200 μg/ml. This data demonstrates that the iron-oxide nanoparticles, whether in free form or co-encapsulated with the nile-red within ormosil nanoparticles, exert negligible toxic effect on the cells. This preliminary experiment indicates that these nanoparticles are non-toxic to cells, and can be used in biological applications.

We have also used fluorescence microscopy of cells treated with the IO-NR/ORM nanoparticles to probe their cellular uptake. The fluorescence of the fluorophore nile-red is used to optically track the doped nanoparticle within the cell. Fig. 6c represents the fluorescence images of the treated cells, showing robust optical signal from the cells (pseudo-coloured in greyscale). The treated cells looked morphologically healthy, further indicating the non-toxicity of particles. Control experiments using untreated cells did not result in any optical signal from cells (Fig. 6b). It may be noted from the above result that efficient optical imaging is possible with a nanoparticle

dosage of 300 ug/ml, which was the lowest dosage used in cell viability studies. These experiments show that the nanoparticles are efficiently uptaken by the cells, thus further highlighting the promise of these nanoparticles as non-toxic optical labels in bioimaging studies.

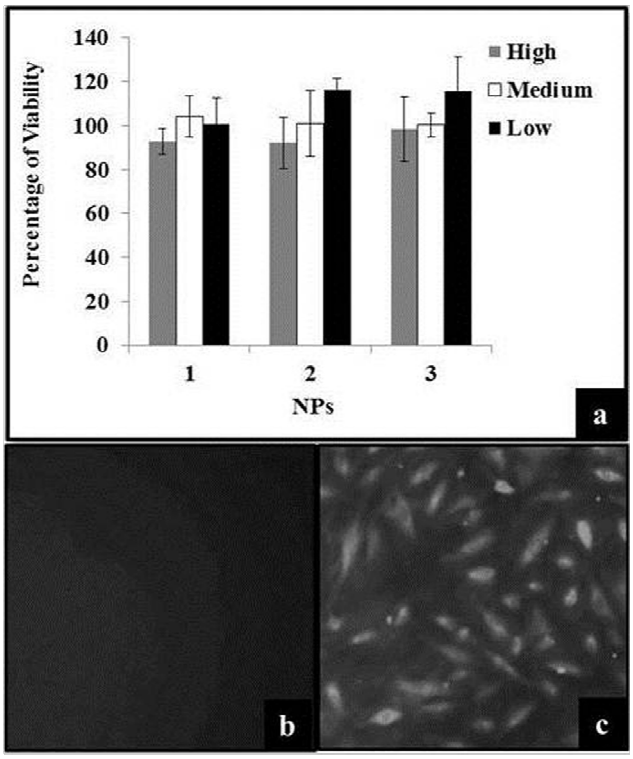


***Fig. 6: (a) Cell viability (MTT) assay probing possible cytotoxic effects of free nile-red (NR, H= 32 µg/mL, M=16 µg/mL, L=8 µg/mL), free iron oxide nanoparticles (IO, H=400 µg/mL, M=200 µg/mL, L=100 µg/mL), and ormosil nanoparticles co-encapsulating iron-oxide nanoparticles and nile-red (IO-NR/ORM, H=1200 µg/mL, M=600 µg/mL, L=300 µg/mL). Average values of three measurements are presented. (b, c) Fluorescence microscopy analysis of MCF-7 cells treated with (b) PBS, and (c) ormosil nanoparticles co-encapsulating iron-oxide nanoparticles and fluorophore NR (IO-NR/ORM). Nanoparticle dosage of 300 µg/mL was used in the bioimaging experiment.***

The above observations of *in vitro* non-toxicity, as well as cellular uptake without the necessity of any active cell-entry strategies, of only fluorophore-doped ormosil nanoparticles were also observed previously; although the size of the particles were much smaller in the previous reports (diameter below 50 nm).[24-30] Their biocompatibility and non-immunogenicity can be attributed to the inertness of the ormosil matrix. The mechanism of their cellular uptake is yet to be determined, though fluid-phase endocytosis is suspected to be the possible route.

## Conclusion

A single probe having magnetic as well as optical properties has the capability to relay both structural (anatomical) and functional (metabolic) bioimaging information. This manuscript highlights the facile synthesis of ormosil nanoparticles co-encapsulating iron-oxide nanoparticles and fluorophore, having both the magnetic and optical properties. Encapsulation of the magnetic nanoparticle within a mesoporous ormosil nanoshell ensures little loss of magnetic resonance imaging (MRI) capability as small water-molecules can freely diffuse across the pores of the ormosil matrix. The MRI capabilities of these nanoparticles will be investigated in detail in the future, along with small animal studies for dual optical and MR imaging *in vivo*. Alongside, detailed biodistribution, biocompatibility and excretion of these nanoparticles *in vivo* will be investigated.

## Acknowledgements

We are grateful to University of Delhi, India, for providing R&D Grant to support this study. We are thankful Dr. Anju Srivastava, Department of Zoology, University of Delhi, for her constructive suggestions with regards to *in vitro* studies. We also thank Mr. Rahul from University Science Instrumentation Center (USIC), University of Delhi, for helping us record TEM images.

## Notes and references

*Department of Chemistry, University of Delhi, Delhi-110007, India. Tel: +91-9560721851; E-mail: indrajitroy11@gmail.com*

† Electronic Supplementary Information (ESI) available: EDX and SAED data. See DOI: 10.1039/b000000x/

1 Paras N. Prasad. Introduction to Nanomedicine and Nanobioengineering, Wiley: New York, 2012.
2 M. L. James and S. S. Gambhir, *Physiol. Rev*., 2012, **92**, 897.
3 L. J. Higgins and M. G. Pomper, *Semin. Oncol*., 2011, **38**, 3.
4 D. E. Lee, H. Koo, I. C. Sun, J. H. Ryu, K. Kim and I. C. Kwon, *Chem. Soc. Rev*., 2012, **41,** 2656.
5 M. Swierczewska, S. Lee and X. Chen, *Mol. Imaging*, 2011, **10**, 3.
6 Y. E. Koo, W. Fan, H. Hah, H. Xu, D. Orringer, B. Ross, A. Rehemtulla, M. A. Philbert and R. Kopelman, *Appl. Opt.*, 2007, **46**, 1924.
7 T. L. Doane and C. Burda, *Chem. Soc. Rev*., 2012, **41**, 2885.
8 P. Sharma, A. Singh, S. C. Brown, N. Bengtsson, G. A. Walter, S. R. Grobmyer, N. Iwakuma, S. Santra, E. W. Scott and B. M. Moudgil, *Methods Mol. Biol*., 2010, **624**, 67.
9 K. T. Yong, I. Roy, M. T. Swihart and P. N. Prasad, *J. Mater. Chem.*, 2009, **19**, 4655.
10 S. Parveen, R. Misra and S. K. Sahoo, *Nanomedicine,* 2012, **8**, 147.
11 S. S. Davis, *Trends. Biotechnol*., 1997, **15**, 217.
12 E. Ruoslahti, S. N. Bhatia and M. J. Sailor, *J. Cell Biol*., 2010, **188**, 759.
13 Y. K. Gong and F. M. Winnik, *Nanoscale*, 2012, 4, 360.
14 J. K. Vasir and V. Labhasetwar, Technol. *Cancer Res.* Treat., 2005, **4**, 363.
15 J. R. McCarthy and R. Weissleder, *Adv. Drug Delivery Rev*., 2008, **60**, 1241.
16 A. K. Gupta and M. Gupta, *Biomaterials*, 2005, **26**, 3995.
17 C. Sun, J. S. H. Lee, and M. Zhang, *Adv. Drug Delivery Rev*., 2008, **60**, 1252.
18 E. Duguet, S. Vasseur, S. Mornet and J. M. Devoisselle, *Nanomedicine (Lond.),* 2006, **1**, 157.
19 D. Ho, X. Sun and S. Sun, *Acc. Chem. Res*., 2011, **44**, 875.
20 L. Levy, Y. Sahoo, K. S. Kim, E. J. Bergey and P. N. Prasad, *Chem. Mater*., 2002, **14**, 3715.
21 M. S. Islam, J. Kurawaki, Y. Kusumoto, M. Abdulla-Al-

Mamun and M. Z. B. Mukhlish, *J. Sci. Res*., 2012, **4**, 97.
22 C. Tassa, S. Y. Shaw and R. Weissleder, *Acc. Chem. Res*., 2011, **44**, 842.
23 S. Das, T. K. Jain and A. N. Maitra, *J. Colloid Interface Sci.,* 2002, **252**, 82.
24 I. Roy, T. Y. Ohulchanskyy, H. E. Pudavar, E. J. Bergey, A. R. Oseroff, J. Morgan, T. J. Dougherty and P. N. Prasad, *J. Am .Chem .Soc*., 2003, **125**, 7860.
25 T. Y. Ohulchanskyy, I. Roy, L. N. Goswami, Y. Chen, E. J. Bergey, R. K. Pandey, A. R. Oseroff and P. N. Prasad, *Nano Lett*., 2007, **7**, 2835.
26 I. Roy, T. Y. Ohulchanskyy, D. J. Bharali, H. E. Pudavar, R. A. Mistretta, N. Kaur and P. N. Prasad, *Proc. Natl. Acad. Sci. U .S. A*., 2005, **102**, 279.
27 R. Kumar, I. Roy, T. Y. Ohulchanskyy, L. N. Goswami. A. C. Bonoiu, E. J. Bergey, K. M. Tramposch, A. Maitra and P. N. Prasad, *ACS Nano*, 2008, **2**, 449.
28 R. Kumar, I. Roy, T. Y. Ohulchanskky, L. A. Vathy, E. J. Bergey, M. Sajjad and P. N. Prasad, *ACS Nano*, 2010, **23**, 699.
29 I. Roy, M. K. Stachowiak and E. J. Bergey, *Nanomedicine*, 2008, **4**, 89.
30 F. Barandeh, P. L. Nguyen, R. Kumar, G. J. Iacobucci, M. L. Kuznicki, A. Kosterman, E. J. Bergey, P. N. Prasad and S. Gunawardena, *PLoS One*, 2012, **7**, e29424.
31 D. P. Yang, F. Gao, D. X. Cui and M. Yang, *Curr. Nanosci*., 2009, **5**, 485.
32 B. L. Bales and M. Almgren, *J. Phys. Chem.* 1995, **99**, 15153.
33 L. M. Rossi, L. Shi, F. H. Quina and Z. Rosenzweig, *Langmuir* 2005, **21**, 4277.
34 A. G. Nasibulin, S. Rackauskas, H. Jiang, Y. Tian, P. R. Mudimela, S. D. Shandakov, L. Nasibulina, J. Sainio and E. I. Kauppinen, *Nano Res*., 2009, **2**, 373.
35 S. Santra, C. Kaittanis, J. Grimm and J. M. Perez, *Small*, 2009, **5**, 1862.

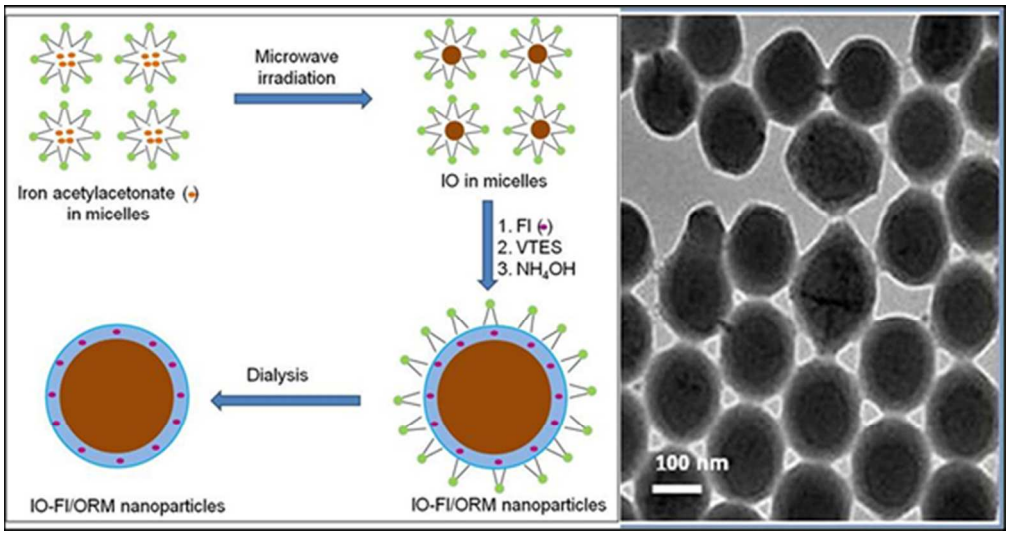


(Left) Scheme depicting formation of ormosil nanoparticles, co-encapsulated with iron-oxide nanoparticles and fluorophore. (Right) TEM image of the synthesized nanoparticles.
75x39mm (300 x 300 DPI)

**Electronic Supplementary Information (ESI)** ***RSC Advances***

# Optically and magnetically doped ormosil nanoparticles for bioimaging: synthesis, characterization, and *in vitro* studies.

Pramod Kumar, Anuradha, and Indrajit Roy

*Department of Chemistry, University of Delhi, Delhi-110007, India.*
*Phone: +91-9560721851*
*E-mail: indrajitroy11@gmail.com*

**Enclosure: Two figures**

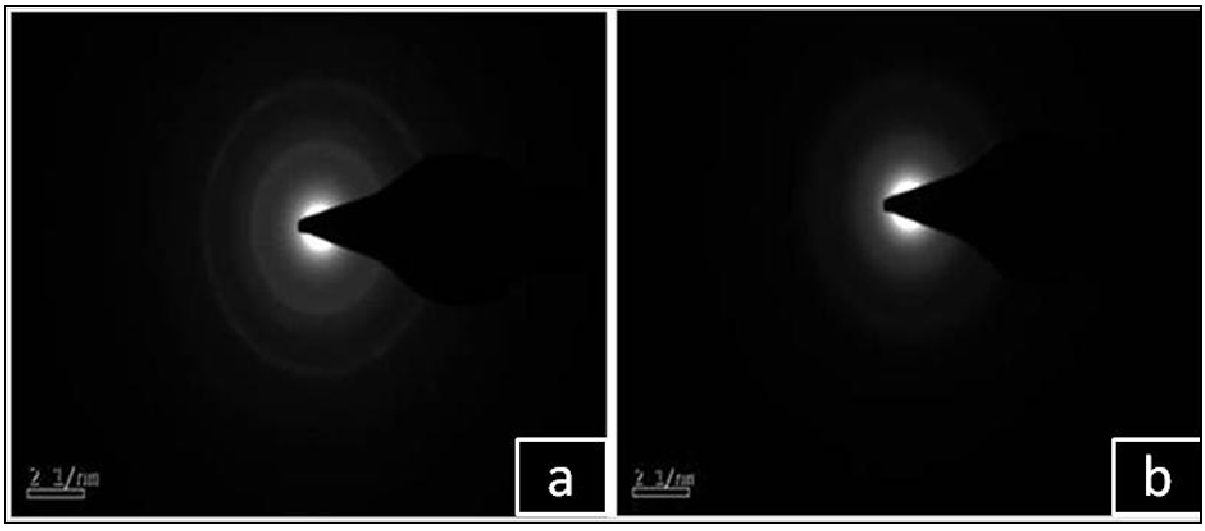


**Fig. S1:** Selected area electron diffraction (SAED) pattern of (a) free iron oxide nanoparticles (IO), and (b) ormosil nanoparticles encapsulating iron-oxide nanoparticles (IO/ORM). The clear diffraction rings visible in (a) appear to be diminished in (b).

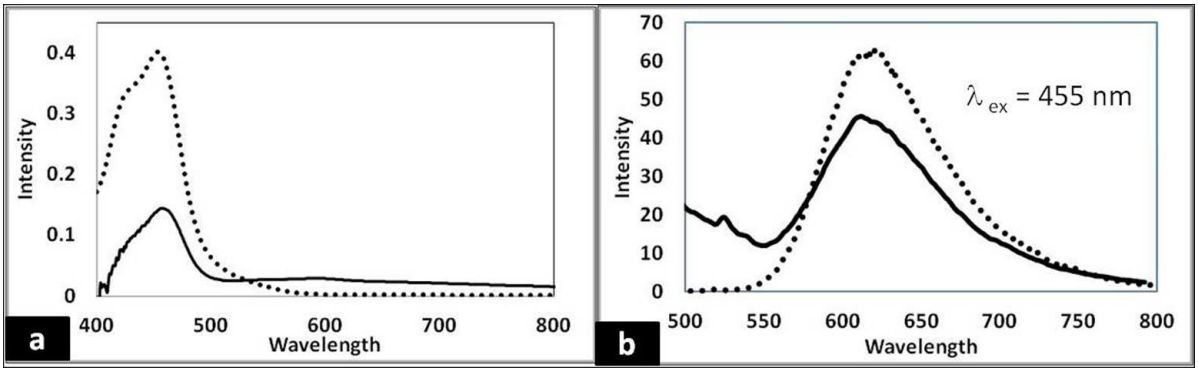


**Fig. S2:** Absorption (a) and fluorescence (b) spectra of fluorophore ruthenium-tris(2,2′-bipyridyl) dichloride (RU), free (broken line) and co-encapsulated with iron-oxide (IO) within ormosil nanoparticles (solid line). The results show that the optical features of the fluorophore are retained, but diminished, upon nanoencapsulation.